# The Impact of Assimilating Precipitation-affected Radiance on Cloud and Precipitation in Goddard WRF-EDAS Analyses

Xin Lin[1], Sara Q. Zhang[1], M. Zupanski[2], Arthur Y. Hou[3], and J. Zhang[3]

[1] Mesoscale Atmospheric Processes Branch
NASA Goddard Space Flight Center, Code 612,
Greenbelt, MD 20771, USA

[2] CIRA/Department of Atmospheric Science
Colorado State University, Fort Collins, CO 80523

[3] Earth Science Division,
NASA Goddard Space Flight Center, Code 610,
Greenbelt, MD 20771, USA

[4] NOAA/National Severe Storms Laboratory
Norman, OK 73072

Submitted to *the Journal of the Atmospheric Sciences*

---

*Corresponding author address:*

Dr. Xin Lin,
Mesoscale Atmospheric Processes Branch,
NASA Goddard Space Flight Center, Code 612,
Greenbelt, MD 20771.

Tel: 301-614-6146
E-mail: xlin.lin-1@nasa.gov

* Additional Affiliation: Earth System Science Interdisciplinary Center, University of Maryland College Park, College Park, Maryland 20742.

## Abstract

High-frequency TMI and AMSR-E radiances, which are sensitive to precipitation over land, are assimilated into the Goddard Weather Research and Forecasting Model-Ensemble Data Assimilation System (WRF-EDAS) for a few heavy rain events over the continental US. Independent observations from surface rainfall, satellite IR brightness temperatures, as well as ground-radar reflectivity profiles are used to evaluate the impact of assimilating rain-sensitive radiances on cloud and precipitation within WRF-EDAS.

The evaluations go beyond comparisons of forecast skills and domain-mean statistics, and focus on studying the cloud and precipitation features in the jointed rain-radiance and rain-cloud space, with particular attentions on vertical distributions of height-dependent cloud types and collective effect of cloud hydrometers. Such a methodology is very helpful to understand limitations and sources of errors in rain-affected radiance assimilations.

It is found that the assimilation of rain-sensitive radiances can reduce the mis-match between model analyses and observations by reasonably enhancing/reducing convective intensity over areas where the observation indicates precipitation, and suppressing convection over areas where the model forecast indicates rain but the observation does not. It is also noted that instead of generating sufficient low-level warm-rain clouds as in observations, the model analysis tends to produce many spurious upper-level clouds containing small amount of ice water content. This discrepancy is associated with insufficient information in ice-water-sensitive radiances to address the vertical distribution of clouds with small amount of ice water content. Such a problem will likely be mitigated when multi-channel multi-frequency radiances/reflectivity are assimilated

over land along with sufficiently accurate surface emissivity information to better constrain the vertical distribution of cloud hydrometeors.

# 1. Introduction

Observing, modeling, and forecasting systems have been undergoing rapid development over the past decade. Satellites are playing an increasingly important role in providing global observations with unprecedented temporal and spatial coverage. With increasing computing powers, general circulation models, by including more physical-based parameterizations on mesoscale effects, are moving toward providing simulations and forecasts at cloud-system-resolving or mesoscale-resolving resolutions (e.g., Putman and Suarez 2011, Jung et al. 2012, Murakami et al. 2012). Cloud-scale-resolving global models –in which the cloud dynamics and mesoscale processes are explicitly resolved instead of being parameterized—also are being actively pursued (e.g., Grabowski 2001; Khairoutdinov and Randall 2001; Randall et al. 2003; Khairoutdinov et al. 2005; Tao et al. 2008). In response to these new developments in both data and models, tremendous efforts have been expended to assimilate high-resolution satellite observations, particularly those related to the hydrologic cycle, into numerical models so that better forecasts and analyses can be achieved for the entire spectrum of weather events as well as flood and landslide.

One of the most challenging and active areas of research and development in data assimilation is to explore effective and efficient approaches to extract the maximum information from error-prone, under-sampled remote sensing of cloud and precipitation processes and benefit model forecasts of the hydrologic cycle. In earlier studies, because of limited knowledge on forecast error covariance associated with clouds and rain and difficulties in constructing suitable observation operators with crude cloud and convection parameterizations, only space-borne observations under the clear-sky

condition (and/or radiation channels insensitive to cloud and precipitation processes) were assimilated in operational models (e.g., Phalippou 1996, Derber and Wu 1998; Gerard and Saunder 1999, Bauer et al 2002, Okamoto and Derber 2006, Kazumori et al. 2008, etc). While this approach is able to improve the large-scale environment and indirectly influences precipitation and cloud via model dynamics and thermodynamics, it is less effective in correcting forecast errors on the hydrologic cycle due to omitting valuable information in cloudy and rainy areas (e.g., Andersson et al 2005; Errico et al. 2007, Zupanski et al. 2011).

Surface rainfall is one of the most important variables that directly link to global water and energy cycle, and a model's moist physics. Significant progress has naturally been made to assimilate satellite rainfall retrievals, particularly those from cloud-penetrating microwave sensors, to explore the benefit of space-borne cloud/precipitation observations on quantitative precipitation forecasts (e.g., Chang and Holt 1994; Tsuyuki 1996a, b, 1997; Fillion and Errico 1997; Xiao et al. 2000; Macpherson 2001; Fllion 2002; Treadon et al. 2002; Tsuyuki et al. 2002; Hou et al. 2004; Moreau et al. 2004; Pu and Tao 2004; Andersson et al. 2005; Mahfourf et al. 2005; Lin et al. 2008). Although assimilations of satellite rainfall retrievals have indicated positive/neutral impacts on forecasts and analyses of the hydrologic cycle in numerical weather prediction (NWP) systems, there are a number of limitations. First of all, data assimilation solutions are corrections on the 3-D atmospheric state variables. Surface rainfall, however, is a 2-D integral quantity containing little information on the vertical structure within cloudy and rainy areas. In order to project the rainfall observation information to the vertical distributions of increments of temperature, humidity and/or hydrometers, assumptions

and simplifications have to be made in the rain observation operator based on physical or empirical parameterizations. Since vertical structure of heating, moistening, and cloud microphysics can be drastically different over convective and stratiform cloud/rain regions as well as in different cases over various climate regimes (e.g., Houze et al. 1981; Houze 1982; Johnson and Young, 1983; Johnson 1984; Hartmann et al. 1984; etc.), these assumptions and simplifications could potentially bring large uncertainties and post significant challenges to operational applications particularly at scales ranging from meso- to cloud scales. Secondly, satellite rainfall estimations are usually derived from retrieval algorithms that employ radiance transfer models, assumptions and sample databases significantly different from those typically used in NWP models. For instance, rain estimations over ocean from PMW imagers are typically derived from physical-based algorithms. The forward model assumptions and a prior databases are often different from those used in global operational models. PMW rain retrievals over land, on the other hand, are still empirically derived based on the statistical relationship between ice water content and surface rain rates. These inconsistencies involving calibration, sampling, and retrieval errors as well as the lack of the "truth" observations make it difficult to estimate rainfall observation errors.

In recent years with the significant advance in developing fast, all-sky radiative transfer models and prognostic cloud models, the direct assimilation of precipitation-affected radiances has shown many promising benefits:

1. As the backbone of space-based precipitation measurements, microwave sensing is able to penetrate clouds and respond to the absorption and scattering of cloud hydrometeor particles. The simultaneous multi-channel, multi-frequency

measurements are able to provide more abundant and physically-consistent information on the vertical structure of hydrometers relative to surface rainfall;

2. Using direct radiance assimilation limits observation errors to only measurement errors, thus effectively avoiding the uncertainty resulted from error sources such as assumptions and simplifications embedded within different rain retrieval algorithms;
3. As radiance forward models, surface emissivity models, and prognostic cloud schemes continue to improve, NWP models combining with fast radiative transfer models can directly calculate cloud- or precipitation-affected radiances, which makes implementations in data assimilation systems straightforward. Observation operators can more directly link the observed radiances with model cloud microphysics.

For example, European Centre for Medium-Range Weather Forecasts (ECMWF) has implemented all-sky radiance assimilation over ocean in the operational global 4DVAR assimilation system (Bauer et al. 2006, 2010; Geer et al. 2010; Geer and Bauer 2011) and demonstrated positive data impact on the analyzed and forecasted dynamic and thermodynamic fields in tropical cyclones and mid-latitude weather systems. Weng et al. (2007) developed a hybrid variational scheme to directly assimilate rain-affected radiances in experiments with the National Centers for Environmental Prediction's Global Data Assimilation System. Their study indicated improved analyses of 3-D temperature structure and wind circulation in hurricane cases.

Multi-channel, multi-frequency, all-sky radiance assimilation represents the future direction for including satellite measurements on cloud and precipitating processes in

data assimilation for NWP at meso- and cloud-resolving scales. NASA Goddard Weather Research and Forecasting model-based Ensemble Data Assimilation System (WRF-EDAS) is designed to assimilate precipitation-affected radiances at cloud-resolving scales to improve analyses on hydrometeors and surface precipitation in numerical predictions (Zupanski et al. 2011). The system takes an ensemble filter approach to obtain flow-dependent forecast error covariance including distinctly different error structure in clear and cloudy regions. It also employs high-resolution forecasting model with explicit cloud microphysics to resolve scales that are comparable with satellite observations. The system performance and data impact have been examined in terms of improvements on forecast skills of storm structure and accumulated surface precipitation (Zhang et al. 2013).

The current work extends the study of Zhang et al. (2013) to further evaluate the impact of assimilating precipitation-affected radiances (85-89 GHz) over land within WRF-EDAS using independent observations. Our analyses and evaluations mainly focus on the statistical distribution of cloud, precipitation, and vertical reflectivity profiles at meso- and cloud-resolving scales. The direct radiance assimilation under cloudy/precipitating conditions is similar to the physical-based maximum likelihood retrieval problem that is constrained by a priori information from model-derived profile uncertainties. The accuracy of estimated hydrometeor profiles determines the forecast skill of consequent surface precipitation. Improvements (or reductions of mis-match) in terms of frequency and intensity of rain events, collective effects of vertical hydrometer profiles, as well as precipitating/non-precipitating cloud types will be examined in more details. Section 2 describes the WRF-EDAS system and assimilation experiments

ingesting rain-affected radiances over land in southeast United States. Section 3 presents observational data and analysis methods, as well as some practical assimilation issues over land that we intend to explore. Section 4 examines statistics in the radiance space over regions where observations indicate rain but the model forecast might not, and where the model forecast shows rain but observations may indicate otherwise. Sections 5 and 6 compare the assimilation results against independent observations of surface precipitation, cloud types and radar reflectivity. Section 7 discusses some potential issues and limitations noted in the evaluation, and presents the final conclusion of the study.

# 2. Assimilation system and experiments

### *2.1 Goddard WRF-EDAS*

Motivated by the scientific goals of Global Precipitation Measuring (GPM) mission (Hou et al., 2011), the Goddard WRF-EDAS has been developed with a focus on utilizing precipitation-affected radiances to produce dynamically-consistent high-resolution precipitation analyses and forecasts (Zupanski et al. 2011, Zhang et al. 2013). The system consists of the Advanced Research version of WRF model (ARW, Skamarock et al. 2005) with NASA Goddard cloud microphysics schemes (e.g., Tao et al. 2003) and longwave and shortwave radiation schemes (Chou and Suarez 1999, 2001), the Maximum Likelihood Ensemble Filter (MLEF: Zupanski 2005, Zupanski et al. 2008), a suite of all-sky radiance observation operators for microwave and radar data derived from Goddard Satellite Data Simulation Unit (GSDSU, Matsui et al. 2009), and the operational data stream of NCEP Grid Point Statistical Interpolation system (GSI, Wu et al. 2002) which includes conventional data and satellite data. In order to explicitly relate the model

cloud microphysics to satellite radiance observations, five prognostic hydrometeors (mixing ratios of rain water, cloud water, snow, ice, and graupel) are included in control variables as well as in the corresponding ensemble-estimated background error covariance. Following Kummerow et al. (1996), the radiative transfer model simulates PMW brightness temperatures under all-sky conditions within the Field of View (FOV) of space-borne instruments.

The ensemble data assimilation scheme in Goddard WRF-EDAS performs the maximum likelihood estimation of atmospheric state by minimizing the discrepancies between model predicted and instrument-measured observables. Unlike the variational method which requires tangent linear models and adjoints of model physical parameterizations, the ensemble method incorporates the full microphysics and radiative transfer in the assimilation procedure and therefore avoids the difficulties in linearization of physical parameterizations on cloud and precipitation processes. The analysis problem is defined as maximum likelihood solutions to the cost function:

$$J(x)=\frac{1}{2}\left(x-x_b\right)^T P_f^{-1}\left(x-x_b\right)+\frac{1}{2}\left[y-H(x)\right]^T R^{-1}\left[y-H(x)\right] \qquad (1)$$

$x$ denotes the control variables consisting of wind, temperature, pressure, water vapor, and hydrometeors. $\boldsymbol{y}$ is the available observation vector and $H(x)$ represents the conversion of model variables into the corresponding observable by the observation operator. The background and observation error covariance are matrix $P_f$ and matrix $R$ respectively. An ensemble of 3-hour model forecasts with perturbations generated from analysis error covariance provides a priori model-derived background information and

estimates forecast error characteristics in $P_f$. In order to assimilate precipitation-affected radiance observations, the WRF-EDAS combines model forecasts with the radiative transfer model of Kummerow et al. (1996) to calculate brightness temperatures for each individual PMW sensors at the model resolution. The simulated brightness temperatures are then convolved within the FOV of PMW sensors through a Gaussian beam pattern. More detailed description on the algorithm and system implementation of Goddard WRF-EDAS can be found in Zhang et al. (2013).

### *2.2 Assimilation experiments using precipitation-affected radiances*

A number of data assimilation experiments are carried out using WRF-EDAS over a 10-day period for a few heavy rain events occurred over the southeast US from 15 UTC, Sep. 12, 2009 to 15 UTC, Sep. 22, 2009. During this period, several persistent low-pressure systems slowly progressed eastward over the Southern US. Organized and scattered rain events dumped significant amount of rainfall from South Central US to Southeast US (Figure 1) and severe flooding was reported across north and central Georgia. The experiment domain is set at 9-km spatial resolutions with 31 model layers from the surface to 50 hPa. The horizontal domain includes 220x168 grid points. The assimilation procedure consists of 32-ensemble-member WRF 3-h forecasts, background error covariance estimation, observation simulation for innovation calculation and non-linear minimization of the analysis equation. The ensemble filter also produces an estimate of the analysis uncertainty that is used to perturb the initial condition for ensemble forecasts in assimilation cycling.

Within the experiment period, two passive microwave sensors, the TRMM Microwave Imager (TMI, Kummerow et al. 1998) and the Advanced Microwave Scanning Radiometer-EOS (AMSR-E) instrument, had 35 and 27 overpasses over the southeast US respectively. These precipitation-affected radiances from TMI and AMSR-E provide a good opportunity to examine the capability of WRF-EDAS in reducing errors in spatial distributions of model cloud and precipitating processes, and to identify potential issues for further system improvement.

TRMM TMI is a nine-channel PMW radiometer measuring radiance at five frequencies ranging from 10.7, 19.4, 21.3, 37 to 85.5 GHz. AMSR-E is one of the six sensors aboard Aqua, which flies in a sun-synchronous orbit. It is a PMW radiometer, measuring brightness temperatures (BT) at 12 channels and 6 frequencies ranging from 6.9 to 89.0 GHz. As shown in Wilheit (1986) and Spencer et al. (1989), high-frequency scattering signals due to ice particles are sensitive to precipitation over land while low-frequency emission signals from liquid particles can be severely contaminated by the land surface emission. Figure 2 shows snapshots of the TMI 85 GHz (V), 37 GHz (V) and 21 GHz (V) overpasses centered at 15Z, September 20, 2009 within the WRF-EDAS experiment domain, along with the observed surface rain rate derived from ground radar and gauge. Clearly, the BT depression at 85 GHz has high correlation with the rainy area over land. At lower frequencies, the BT difference between the raining area and the background becomes smaller and the weak BT depression appears to be insensitive to rain intensities. It is for this reason that the current retrieval algorithms typically use high frequency channels to empirically estimate surface precipitation over land.

Two assimilation experiments are examined in the study. The control experiment (CNTR-exp) assimilates the conventional data and clear-sky sounder brightness temperatures. The precipitation experiment (PRCP-exp) assimilates TMI and AMSR-E precipitation-affected radiances in addition to the conventional and clear-sky data. To identify precipitation pixels using low- and high frequencies from both observations and in simulated BT, a scattering index over land (SIL) following Wilheit et al. (2003) is calculated as a measure of BT depression due to scattering by precipitation:

SIL=451.9-0.44*Tb(19v)-1.775*Tb(22v)+0.00575*Tb(22v**2-Tb(85v)

For any locations where the SIL value is larger than 10K, the radiance is identified as a precipitation-affected radiance. Since the focus of the experiments is over land, high-frequency radiances of TMI 85 GHz and AMSR-E 89 GHz are assimilated in PRCP-exp, while measurements at lower frequencies are only used in the SIL index calculation and in passive monitoring process.

## 3. Data and Analysis Methodologies

Three data sets are used in the evaluation of the cloud and precipitation distributions in the WRF-EDAS analyses: ground-based surface rainfall estimates, satellite IR brightness temperatures for cloud top information, and radar reflectivity for vertical hydrometeor structure.

The surface rainfall data used in this study are the merged surface radar and rain gauge product from the NCEP National Hourly Multi-Sensor Precipitation Analysis Stage IV (Lin and Mitchell 2005). This data set collects hourly radar rainfall estimates

from about 140 WSR-88D operational radars over the US continent, merging with about 3000 hourly gauge reports. The Stage IV data are preliminarily quality controlled and calibrated. It covers the entire US continent at 1-h intervals from 2002 to the present. Although it is understandable that there might still be some uncertainties on issues such as data quality and calibration, this dataset offers an independent observation-based surface rainfall estimate at fine temporal and spatial resolutions, with continuous sampling of various rain events over the continental US. The precipitation product is on an 1121x881 polar stereographic grid, and is at the 4-km resolutions. The data are mapped onto 9-km grid spacing for evaluating WRF-EDAS output. In order to obtain an estimation of cloud coverage and cloud top and collocate them with precipitating areas, Level-1 brightness temperature data from the TRMM Visible and Infrared Scanner (VIRS) are also used. The thermal infrared wavelength at 12.0 micron allows a determination of cloud top height and cloud top temperature.

The observed vertical reflectivity profiles used in this study are from the National Mosaic and Multi-sensor QPE (Quantitative Precipitation Estimation), or “NMQ”, system (Zhang et al. 2011). The system ingests base level data from over 140 WSR-88D S-band radars and about 31 Canadian C-band weather radars and generates 3-D radar reflectivity mosaic and QPE products. This invaluable radar dataset, with 1-km horizontal resolutions covering the entire United States and southern Canada at 5-minute time intervals, offers us an excellent opportunity to examine detailed transient features at synoptic-, meso-, and cloud-resolving scales.

Model forecasts and analyses typically do not match exactly with radiance/rainfall observations in terms of intensity and coverage. This is especially conspicuous at meso-

and cloud-resolving scales. Figure 3 is an example of a typical scene in which the model forecast (or the first-guess) and the observation have large mismatches. Even in the overlapped region, there could still be large differences in rain/radiance intensity and in vertical distributions of cloud hydrometers. Here the "clear" area on the background refers to the rain-clear region instead of the cloud-clear region since the high-frequency scattering signals from PWM sensors are only sensitive to precipitation-affected radiance over land. Apparently the domain-averaged statistics may not be an effective approach because of possible large cancellations and of changes in the vertical distribution. In order to examine in detail the impact of assimilating precipitation-affected radiances on cloud and precipitation, we categorize the model domain into 3 regions: (1) Clear (neither the observation nor the model forecast indicates rain); (2) The observation indicates rain; (3) The model forecast shows rain. As a first step we use histograms and jointed histograms to examine the impact of assimilating precipitation-affected radiances on precipitation and cloud within WRF-EDAS. We are particularly interested in looking at the following questions:

- What is the statistical relationship between rain intensity spectra over land and high-frequency scattering signals in observations?
- Can the analysis, after assimilating rain-sensitive radiance, produce more consistent rainfall-cloud distributions than the first guess, or at least moving toward to the right direction in the rain-radiance-cloud space?
- What is the data assimilation impact in regions where the observation suggests rain but the model forecast may not, and *vice-visa,* especially on the vertical

distributions of cloud hydrometers? How does the population of precipitating/non-precipitating clouds vary?

In addition, the high-frequency scattering signals over land have most contributions from frozen particles in the middle to upper troposphere. Can the data assimilation propagate the observation information vertically through the background error covariance and have impacts on the population of warm-rain clouds at lower levels?

## 4. The Radiance Space

Before examining the assimilation impact in the jointed rain-radiance and rain-cloud space, it is worthwhile to first look at the response of radiance assimilation over raining areas at different PMW frequencies. Figure 4 shows the normalized probability distribution function (PDF) of radiances at 85, 37, and 19 GHz (both in vertical and horizontal polarizations) for TMI observations, first-guess and analysis over regions where Stage IV rainfall observations are larger than 1.0 mm/hr. The rain rate threshold is selected to unambiguously distinguish the raining area because the minimum detectable rain rate for PMW imagers is estimated to be around 1.0 mm/hr over land.

Among all the PDFs shown in Figure 4, the first guess and analysis at 85 GHz indicate moderate changes in both vertical and horizontal polarizations. As the frequency becomes lower, the difference between the first-guess and analysis becomes smaller, indicating that the changes in hydrometer profiles are more sensitive to high-frequency scattering signals over land, and less sensitive to low-frequency signals. It is noted that the radiance PDF in first-guess and analysis are of very little difference at 19 GHz.

Therefore in the following discussions, only the results of high-frequency radiance are discussed unless specifically mentioned.

As shown in Wilheit (1986) and Spencer et al. (1989), ice generally only scatters microwave radiation, and scattering tends to increase with frequency and with rain rate. Typically the lower the high-frequency radiance value, the more ice water content in the atmosphere and more likely the heavier the surface rain rate. At 85 GHz, TMI radiance over the observed raining area (> 1 mm/hr.) indicates a single, weak PDF peak (16%) centered near 284 K, and the percentage value gradually decreases as radiance becomes lower. The observed 85 GHz radiance distributions appear to be consistent with what shown in Figure 1 that light, moderate, and heavy rain samples co-existed in the series of organized and scattered rain events during the 10-day period. Both the model first-guess and analysis, however, indicate strong single PDF peaks centered at 291 K (about 45% and 36% respectively) with most radiance samples between 280 K and 300 K, suggesting that there are a significantly large number of samples with little ice water content in model results. Since the contribution of radiance at the top of the atmosphere comes from the atmosphere and the land surface. It is possible that many of large values are scattering signals from the land surface. These large PDF departures from the TMI results are indications of significant mismatches between model results and observations. After precipitation-affected radiance assimilation, it is apparent that the analysis tends to increase the number of samples between 270 and 285 K, and decrease the number of samples above 287 K. Although not significant, the analysis indeed moves toward being more consistent with TMI radiance observations.

# 5. The Rain-Cloud-Radiance Space

### *5.1 Over areas where observations indicate rain*

Figure 5 illustrates jointed histograms in the rain-radiance space for all collocated samples over region where Stage IV surface radar-gauge data indicate rain (rain rate > 0. mm/hr.). Coincident observations on TMI radiance (85 GHz) and surface rain rate (Fig. 5a) indicate a large number of samples concentrating above 270 K, with rain rates ranging from 0.1 to 4 mm/hr. As will be demonstrated in Figure 6, many of these samples are associated with warm-rain processes with almost no ice phases involved and their rain intensities generally do not correlate with Tb (85 GHz). Excluding the above samples with rain rates < 4 mm/hr and with Tb (85 GHz) > 270 K, most other samples tend to follow the general pattern shown in Wilheit (1986) and Spencer et al. (1989): the colder the 85 GHz Tb, the more likely the heavy surface precipitation. On the other hand, we can notice a number of heavy-precipitating samples corresponding with warm 85 GHz Tb, suggesting that warm-rain processes can also occasionally precipitate heavily. There are also some light-precipitating samples corresponding with moderately cold 85 GHz Tb (between 230 K and 270 K). These samples are probably associated with dissipating anvil clouds generated from major convective systems. Although they contain considerable amount of ice water content, precipitation reaching the surface is generally light due to strong evaporation at low levels.

Because of mismatches, the model first guess (FGS, Fig. 5b) tends to have many samples with colder Tb over areas where observations only indicate light to intermediate rain rates. At the meantime, there are also a significant number of FGS samples with Tb around 290 K. These very warm radiances likely indicate dominant contributions from

very shallow clouds and/or land surface under the clear-sky condition, but they inconsistently collocate with observations of considerably large rain rates. The analysis (ANA, Fig. 5c) tends to modify the inconsistency in histograms of model radiances and observed surface rain rates. As shown in Figure 5d, the analysis tends to reduce the number of samples of very cold radiance over areas where observations indicate light to moderate precipitation rates. At the same time, the number of samples with very warm BT values is significantly reduced. The analysis shows more samples with radiance values between 260 K and 285 K, an indication of an increasing population of clouds with more hydrometeor contents. For rain events at moderate and heavy rain intensities, the frequency distribution of model analysis radiance is in better agreement with observations.

To further explore the correlation between TMI high-frequency signals and precipitating clouds involving ice and liquid-only processes, we partition the TMI 85 GHz radiances into four groups and examine their statistical distributions in the rain-cloud-top height space. This practice will help to better illustrate the impact of rain-sensitive radiance assimilation on height-dependent cloud types over land. Figure 6 shows accumulated distributions of TMI 85 GHz radiances on jointed histograms of surface radar-gauge rain rate and VIRS 12μm brightness temperature. The VIRS thermal infrared data can be approximately used to estimate cloud-top temperature/height. The dashed line and the dotted line in the horizontal represent the 0°C level (273 K) and -20°C level (253 K), respectively. The layer between 253 K and 273 K is usually defined as the mixed-phase layer where ice and liquid phases can coexist.

For samples with 85 GHz TMI radiances greater than 270 K, precipitating cloud tops can range from low, middle, to upper levels but low- and middle-level clouds dominate the raining cloud population. There is a clear cloud population peak between 280 K and 290 K corresponding to about 2-4 km above the ground. Light-moderate precipitation is mainly produced by low- and middle-level clouds with cloud top height below 0° C level or nor far above it. Considering that some precipitating clouds overshooting the 0° C level may not involve ice-phase changes either, we could argue that the warm-rain process has an important contribution to the precipitation frequency of occurrence, particularly for rain intensities below 2.0 mm/hour. This is the area where the PMW land rainfall retrieval has significant challenges. For samples with TMI radiances between 250 K and 270 K, most raining clouds have their cloud tops above the melting level and there is a sample peak with cloud tops between 230 K and 240 K which correspond to about 10-12 km above the ground. There are also considerable middle-level precipitating clouds with tops within the mixed-phase layer. For samples with TMI radiances smaller than 250 K, almost all the precipitating clouds have their cloud tops above the -20°C level and involve ice-phase changes. Most of their corresponding surface rain rates are above 1.0 mm/hour. The colder the 85 GHz brightness temperatures and the higher the cloud top height, the heavier the precipitation.

Figure 7 shows the corresponding cloud population of different FGS 85 GHz radiance ensembles as forecasted by the model over the area where observations indicate rain. Here the model simulated 12μm brightness temperatures are estimated based on algorithms developed by Nakajima and Tanaka (1986, 1988). Because of mismatches, the model forecast shows a double-peak cloud-top distribution in the vertical for FGS

radiances greater than 270 K. The major one is between 285 K and 295 K suggesting a significantly overestimated shallow cloud population (and/or ground features) at low levels. In the upper troposphere between 220 K and 240 K, there is also a minor peak likely associated with dissipating anvil clouds and/or high cloud debris. For FGS BT less than 270 K, the middle- and high-level cloud population is not only very small, but also located over areas where observations indicate light to moderate rain rates.

After assimilating 85 GHz TMI radiances, the difference plot (ANA-GFS) in Figure 8 indicates that for model samples with radiances greater than 270 K, the overestimated shallow cloud population in first guess is significantly reduced. The analysis is in better agreement with observations below the 0°C level. We can also notice a small increase of middle-level clouds over areas where the observed rain rates are light or moderate, and a small reduction of middle- and upper-level clouds over areas where the observed rain rates are large. Besides the above changes, there is also a large increase of clouds with small amount of ice water content but topping between 200 K and 220 K, which is inconsistent with observations.

For samples with radiances less than 230 K, the population of deep cloud with large ice water content is reasonably reduced over regions where observations only indicate light rain intensities. However, the analysis is not able to increase the population of deep clouds over areas where observations show moderate to heavy precipitation. On the other hand, for samples with radiances between 230 K and 250 K, the analysis does show a reasonable reduction of deep clouds over light-rain areas and an increase of deep clouds over moderate-to-heavy rain areas. For samples with 85 GHz radiances between

250 K and 270 K, the analysis indicates a general increase of deep clouds over raining areas, similar to observations although the cloud tops are a little higher.

In summary, over the area where observations indicate abundant rainfall coming from both deep convection and frequent warm-rain processes, the model forecast however shows a scene not favorable to vigorous convection, with a dominant population of very shallow clouds (and/or land surface) along with some dissipating high clouds. After assimilating 85GHz radiances, the rain-cloud distribution of model analysis is more consistent with observations than that of the first guess. The overestimated shallow cloud population near the surface is significantly reduced. The statistics of cloud population with considerably large ice water content (radiances < 270 K) also indicates reasonable improvements at upper levels for different rain intensities. However, instead of greatly enhancing warm-rain processes as shown in observations, the model analysis tends to generate many spurious upper-level clouds with small amount of ice water content. This discrepancy possibly reflects limitations in the current model error covariance: there could be different height-dependent cloud types corresponding to the same warm 85 GHz radiance, but the assimilation scheme has little information to further constrain their vertical distributions.

### *5.2 Over areas where the model forecast indicates rain*

In order to examine how effective the rain-sensitive radiance assimilation can indirectly suppress and remove convection, Figure 9 shows accumulated distributions of 85 GHz radiances over areas where the model forecast indicates precipitation but the observation shows zero rain. Observations clearly show that most samples over the area

have radiance values greater than 280 K. In contrast, the model forecast suggests considerably more samples with moderate to large ice water content. After radiance assimilation, the analysis is in better agreement with observations: samples with moderate to large ice water content are reduced, and samples with small or little ice water content are significantly increased.

Partitioning 85 GHz radiance data into 4 groups based on their ice water content, and presenting the statistics in the rain vs. cloud-top height space, we can clearly notice (Figure 10) that the observation shows a dominant shallow cloud population, along with some middle- to upper-level clouds but with small ice water content. There are few deep clouds with large ice water content over the area where the model forecast indicates rain but the observation does not. On the other hand, the model forecast (Figure 11) shows frequent occurrence of deep convection containing moderate-to-large amount of ice water content. In addition, there is a major peak at low levels for samples with radiance values greater than 270 K, suggesting a dominant shallow cloud population featuring warm-rain processes. After radiance assimilation, the difference plot in Figure 12 shows that the deep cloud population with considerably large amount of ice water content is reduced in the analysis. For samples with BT between 250 K and 270 K, their corresponding cloud-top heights become lower. These changes, although small, are consistent with observations. For samples with BT greater 270 K, the shallow cloud population is reasonably reduced. However, clouds with their tops at middle and upper-levels are erroneously enhanced. These discrepancies are again associated with insufficient information contained in high-frequency radiance data to address the vertical distribution of clouds with small amount of ice water content.

# 6. The Impact on Reflectivity Profiles

Although 5 prognostic hydrometeors (mixing ratios of rain water, cloud water, snow, ice, and graupel) are included in analysis control variables, it is difficult to directly evaluate the impact of radiance assimilation on individual hydrometer profiles because of the lack of observations. In addition, averaging hydrometer profiles over large domains usually involves large cancellations, thus providing limited information in both horizontal and vertical directions. One indirect approach, typically used in cloud model evaluations and radar observational studies, is adopted here to compare the statistics of vertical reflectivity profiles in both observations and model results, so that the collective impact of rain-sensitive radiance assimilation on vertical hydrometer profiles can be examined.

The methodology of Contoured Frequency with Altitude Diagram (CFAD: Yuter and Houze 1995) of radar reflectivity is used to compare model results with observations. Observed radar CFADs are calculated from NMQ S-band radar reflectivity averaged onto the WRF model resolutions. Modeled S-band radar reflectivity is first estimated using the ground radar simulator (Masunaga and Kummerow 2005) in NASA GSDSU, and then radar CFADs are computed for FGS and ANA respectively.

Figure 13 shows CFADs of observed and simulated radar reflectivity, as well as the difference between FGS and ANA over the area where observations indicate rain. The observed CFAD indicates that the highest frequency of radar reflectivity is located between 10 and 13 km with reflectivity values around 5-10 dBZ. The contours have a relatively narrow distribution at upper levels. Below the freezing level, the CFAD exhibits a broad distribution with the second highest frequency of radar reflectivity below

2 km with reflectivity values centering between 20 and 25 dBZ. The frequency distribution of observed radar reflectivity is consistent with analyses shown in the rain-cloud-radiance space. The FGS CFAD is however quite different from the observed, with a broad distribution at all levels. The highest frequency of radar reflectivity is located at both upper and low levels, with most reflectivity values below 5 dBZ suggesting a less convective scene comparing with observations. After assimilating 85 GHz radiance, there is an increase in frequency of low reflectivity values (0-5 dBZ), and a decrease in frequency of high reflectivity values (15-30 dBZ) between 5 and 12 km. The frequency contours become more packed above the freezing level. Below 3 km, an increase in frequency of reflectivity can be noticed with reflectivity values centering between 8 and 15 dBZ. Although these vertical changes are small, they are clearly moving in the right direction and try to enhance model convection to better match with observations.

Over the area where FGS indicates rain but observation shows zero rain (Figure 14), the observed CFAD generally shows a less convective feature with a narrow distribution at all levels and most reflectivity values are below 10 dBZ. The highest frequency of radar reflectivity is located at upper levels between 12 and 14 km with reflectivity values centering at 5 dBZ. At low levels, there is also a second peak near the surface with reflectivity values below 5 dBZ. The FGS CFAD has a double-mode structure in both upper and low levels, similar to the observed. But it has a broader distribution (loose contours), particularly above the freezing level. After the radiance assimilation (ANA-FGS), the frequency of high radar reflectivity is reduced in the vertical, while the frequency of low radar reflectivity is enhanced. The ANA CFAD tends to have a narrower distribution than the FGS CFAD. Overall, the rain-sensitive radiance

assimilation appears to reduce the convective intensity (and/or hydrometer contents) in FGS, and pushes ANA to be statistically in a better agreement with observations in the vertical.

## 7. Discussions and Summary

Assimilation of multi-channel, multi-frequency radiance observations on the hydrologic cycle represents one of the most promising directions for including remote-sensing measurements on the vertical structure of cloud and precipitation processes in atmospheric data assimilation to produce better forecasts and analysis at global, cloud-resolving scales. To explore effective pathways to achieve these ultimate goals, the Goddard WRF-EDAS has been developed to utilize precipitation-sensitive radiances at meso- and cloud-resolving scales. This work extends the study of Zhang et al. (2013) to further analyze the data impact of high frequency 85 and 89 GHz radiances from TMI and AMSR-E, which are sensitive to precipitation over land, on a series of rain events over the continental US. Independent observations from ground-based radar and gauge merged rainfall, satellite IR brightness temperatures, as well as ground-radar vertical reflectivity profiles are used to evaluate the impact of assimilating rain-sensitive radiance on cloud and precipitation statistics within WRF-EDAS.

Our analyses and evaluations go beyond comparisons of forecast skills and domain-mean statistics, and focus on studying the cloud and precipitation features in the jointed rain-cloud and rain-radiance space, as well as frequency distributions of vertical reflectivity profiles. These methodologies effectively avoid the large cancellation and potential ambiguities in addressing observation-model mis-matches in rain/clear areas.

Improvements (or reductions of mis-matches) in terms of frequency and intensity of rain events, height-dependent precipitating cloud population, as well as collective effects of vertical hydrometer profiles are examined in details over areas where the observations indicates rain, and over areas where the model forecast indicates rain but the observation does not. Sources of uncertainties are categorized and characterized in order to provide clear physical interpretations on the forecast skill and domain-mean statistics, especially on the capability and effectiveness of the assimilation scheme in enhancing and suppressing precipitating processes at various scales.

Over the area where observations indicate abundant rainfall coming from both deep convection and frequent warm-rain processes, the model first guess, because of mismatches, shows a dominant population of very shallow clouds (and/or land surface) along with some dissipating high clouds. Assimilation of 85-89 GHz radiances reduces the mis-matches between the observed rain rate and collocated model 2-D quantities such as radiances simulated from analyses of hydrometeors. The analysis tends to significantly reduce the number of samples of very warm radiances and increase the number of samples with radiance values between 260 K and 285 K. In addition, the number of samples with very cold radiances is reduced over areas where observations indicate light to moderate precipitation rates. Over areas where observations indicate heavy rain, although there are almost no changes in the number of sample with very cold radiances, the number of samples with smaller amount of ice water content does increase, suggesting some degrees of convective enhancement in the analysis due to the radiance assimilation.

By partitioning collocated samples into 4 radiance categories and studying the vertical distribution of the height-dependent cloud population containing different amount of ice water content, we found that the model-overestimated shallow cloud population near the surface is significantly reduced after radiance assimilation. The statistics of cloud population with considerably large amount of ice water content (radiances < 270 K) also indicates reasonable improvements at middle and upper levels for different rain intensities. These features are consistent with the improvement shown in CFAD of vertical reflectivity profiles. However, instead of greatly enhancing warm-rain processes as shown in observations, the model analysis tends to generate many spurious upper-level clouds with small amount of ice water content. This discrepancy reflects limitations in the current background error covariance: there could be different height-dependent cloud types corresponding to the same warm 85 GHz radiance, but the assimilation scheme has little information to further constrain their vertical distribution.

Over the area where the model forecast indicates rain but the observation does not, the rain-sensitive radiance assimilation helps to suppress and remove convection by either reducing the deep cloud population with large ice water content and/or lower cloud top heights for clouds with moderate ice water content. However, although the shallow cloud population with BT greater than 270 K is reasonably reduced, clouds with their tops at middle and upper-levels are erroneously enhanced. These discrepancies are again associated with insufficient information contained in high frequency radiance data and the limited accuracy of background error covariance particularly in vertical error correlations to address the vertical distribution of clouds with small amount of ice water content.

The present study has examined the impact of assimilating narrow-band, frozen-particle-sensitive radiances on statistics of cloud and precipitation over land within a regional mesoscale ensemble data assimilation system—Goddard WRF-EDAS. The capability and limitation of assimilating ice-water-sensitive radiances in redistributing cloud/precipitation processes involving low amount of ice water content are investigated. The resulted erroneously enhanced cloud population at middle and upper levels, if not well constrained, could affect model cloud and radiation calculations which eventually leads to large errors in model hydrologic predictions. We expect that such a problem could be mitigated when multi-channel multi-frequency radiances/reflectivity can be assimilated over land with sufficiently accurate surface emissivity information to better constrain the vertical distribution of cloud hydrometers. Further studies are being planned to explore impact of simultaneously assimilating rain-sensitive radiance and reflectivity data on cloud and precipitation within WRF-EDAS. The connection and impact between model cloud microphysics and ensemble forecast-based background error covariance in hydrometeors will be studied to improve the vertical error correlations. The changes of the convective and stratiform precipitation regions, which feature different cloud microphysics, will also be investigated.

***Acknowledgements***

The NCEP surface radar and gauge Stage IV data are obtained from National Center for Atmospheric Research Earth Observing Laboratory. The TRMM VIRS radiance data are obtained from NASA Goddard Earth Sciences Data and Information Services Center. The NMQ vertical reflectivity data are obtained from NOAA National Severe Storm Laboratory. We thank Dr. T. Matsui (University of Maryland ESSIC/NASA GSFC) for providing help with the Goddard satellite data simulator unit. This research was supported by the GPM project at the NASA GSFC in Greenbelt, MD.

# References

Andersson, E., and coauthors, 2005: Assimilation and modeling of the atmospheric hydrological cycle in the ECMWF Forecasting System. *Bulletin of the American Meterological Society*, 86, 387-402.

Bauer, P., P. Lopez, A. Benedetti, D. Salmond, S. Saarinen, and M. Bonazzola, 2006: Implementation of 1D+4D-Var assimilation of precipitation-affected microwave radiances at ECMWF. Part II: 4D-Var. *Quart. J. Roy. Meteor. Soc*., 132, 2307-2332.

Bauer, P., G. Kelley, and E. Andersson, 2002: SSM/I radiance assimilation at ECMWF. Proc. *ECMWF/GEWEX Workshop on Humidity Analysis*, Reading, United Kingdom, ECMWF, 167-175.

Bauer, P., A. J. Geer, P. Lopez, D. Salmond, 2010: Direct 4D-Var assimilation of all-sky radiances. Part I: Implementation. *Quart. J. Roy. Meteor. Soc*., 136, 1868-1885.

Chang, S. W., and T. R. Holt, 1994: Impact of assimilating SSM/I rainfall rates on numerical prediction of winter cyclone. *Mon. Wea. Rev*., 122, 151-164.

Chou, M.-D., and M. J. Suarez, 1999: A solar radiation parameterization for atmospheric studies. NASA Tech. Rep. NASA/TM-1999-10460, vol. 15, 38pp.

Chou, M.-D., and M. J. Suarez, 2001: A thermal infrared radiation parameterization for atmospheric studies. NASA Tech. Rep. NASA/TM-2001-104606, vol. 19, 55pp.

Derber, J. C., and W.-S. Wu, 1998: The use of TOVS cloud-cleared radiances in the NCEP SSI Analysis System. *Mon. Wea. Rev*., 126, 2287-2299.

Errico, R., P. Bauer, J.-F. Mahfouf, 2007: Issue regarding the assimilation of cloud and precipitation data. *J. Atmos. Sci*., 64, 3785-3798.

Fillion, L., 2001: Variaitional assimilation of precipitation data and gravity wave excitation. *Mon. Wea. Rev*., 130, 357-371.

Fillion, L., and R. Errico, 1997: Variational assimilation of precipitation data using moist convective parameterization schemes: A 1D-Var study. *Mon. Wea. Rev*., 125, 2917-2942.

Geer, A. J., P. Bauer, and P. Lopez, 2010: Direct 4D-Var assimilation of all-sky radiances. Part II: Assessment. *Q. J. Roy. Meteor. Soc*., 136, 1886-1905.

Geer, A. J. and P. Bauer, 2011: Observation errors in all-sky data assimilation. *Quart. J. Roy. Meteor. Soc*., 137, 2024-2037.

Gerard, E., and R. W. Saunders, 1999: 4DVar assimilation of SSM/I total column water vapor in the ECMWF model. *Quart. J. Roy. Meteor. Soc*., 125, 3077-3101.

Grabowski, W. 2001: Coupling cloud processes with the large-scale dynamics using the cloud-resolving convection parameterization (CRCP). *J. Atmos. Sci*., 58, 978-997.

Hartmann, D. L., H. H. Hendon, and R. A. Houze, Jr., 1984: Some implications of the mesoscale circulations in tropical cloud clusters for large-scale dynamics and climate. J. Atmos. Sci., 41, 113-121.

Hou, A., Y., S. Q. Zhang, and O. Reale, 2004: Variational continuous assimilation of TMI and SSM/I rain rates: Impacts on GEOS-3 hurricane analyses and forecasts. *Mon. Wea. Rev.*, 132, 2094-21-9.

Hou, A. Y., and Co-authors, 2011: The Global Precipitation Measurement (GPM) Mission. Conditionally accepted by *Bulletin of the American Meteorological Society*.

Houze, R. A., Jr., S. G. Geotis, F. D. Marks, and A. K. West, 1981: Winter monsoon convection in the vicinity of North Borneo. Part I: Structure and time variation of the clouds and precipitation. Mon. Wea. Rev., 109, 1595-1614.

Houze, R. A., Jr., 1982: Cloud clusters and large-scale vertical motuons in the tropics. J. Meteor. Soc. Japan, 60, 396-409.

Johnson, R. H., and G. S. Young, 1983: Heat and moisture budgets of tropical mesoscale anvil clouds. *J. Atmos. Sci*., 40, 2138-2147.

Johnson, R. H., 1984: Partitioning tropical heat and moisture budgets into cumulus and mesoscale components: Implications for cumulus parameterization. *Mon Wea. Rev*., 112, 1590-1601.

Jung, T., and Co-authors, 2012: High-resolution global climate simulations with the ECMWF model in Project Athena: Experimental design, model climate, and seasonal forecast skill. *Journal of Climate*, 25, 3155-3172.

Kazumori M., Q. Liu, R. Treadon, and J. C. Derbet, 2008: Impact study of AMSR-E radiances in the NCEP Global Data Assimilation System. *Mon. Wea. Rev*. 136, 541-559.

Kharoutdinov, M. F., and D. A. Randall, 2001: A cloud resolving model as a cloud parameterization in the NCAR Community Climate System Model: Preliminary results. *Geophys. Res. Lett*., 28, 3617-3620.

Kharoutdinov, M. F., D. A. Randall, and C. Demott, 2005: Simulation of the atmospheric general circulation using a cloud-resolving model as a superparameterization of physical processes. *Journal of the Atmospheric Sciences*, 62, 2136-2154.

Kummerow, C., W. S. Olson, and L. Giglio, 1996: A simplified scheme for obtaining precipitation and vertical hydrometeor profiles from passive microwave sensors. *IEEE Trans. Geosci. Remote Sens*., 34, 1213-1232.

Kummerow, C., W. Barnes, T. Kozu, J. Shiue, and J. Simpson, 1998: he Tropical Rainfall Measuring Mission (TRMM) sensor package. *J. Atmos. Oceanic Technol*., 15, 809-817.

Lin, X., S. Q. Zhang, and A. Y. Hou, 2008: Variation assimilation of global microwave rainfall retrievals: Physical and dynamical impact on GEOS analyses. *Mon. Wea. Rev*., 135, 2931-2957.

Lin, Y., and K. E. Michell, 2005: The NCEP Stage II/IV hourly precipitation analyses: development and application. Preprints, 19th Conf. On Hydrology, American Meteorological Society, San Diego, CA, 9-13 January 2005, P. 1-2.

Macpherson, B., 2001: Operational experience with assimilation of rainfall data in the Met Office mesoscale model. *Meteor. Atmos. Phys*., 76, 3-8.

Mahfouf, J.-F., P. Bauer, and V. Marecal, 2005: The assimilation of SSM/I and TMI rainfall rates in the ECMWF 4D-Var system. *Quart. J. Roy. Soc*., 131, 437-458.

Masunaga, H., and C. D. Kummerow, 2005: Combined radar and radiometer analysis of precipitation profiles for a parametric retrieval algorithm. *J. Atmos. Oceanic Technol*., 22, 909-929.

Matsui, T., X. Zeng, W.-K. Tao, H. Masunaga, W. S. Olson, and S. Lang, 2009: Evaluation of long-term cloud-resolving model simulations using satellite radiance observations and multifrequency satellite simulators. *Journal of Atmospheric and Oceanic technology*, 26, 1261-1274.

Moreau. E., P. Lopez, P. Bauer, A. M. Tompkins, M. Janiskova, and F. Chevallier, 2004: Variational retrieval of temperature and humidity profiles using rain rates versus microwave brightness temperature. *Quart. J. Roy. Meteor. Soc*., 130, 827-852.

Murakami, H., and Co-authors, 2012: Future changes in tropical cyclone activity projected by the new high-resolution MRI-AGCM. *Journal of Climate*, 25, 3237-3260.

Nakajima, T., and M. Tanaka, 1986: Matric formulations for the transfer of solar radiation in a plane-parallel scattering atmosphere. *J. Quant. Spectrosc. Radiat. Transfer,* 35, 13-21.

Nakajima, T., and M. Tanaka, 1988: Algorihms for radiative intensity calculations in moderately thick atmospheres using a truncation approximation. J. Quant. Spectrosc. Radiat. Transfer, 40, 51-69.

Okamoto, K., and J. C. Derber, 2006: Assimilation of SSM/I radiances in the NCEP Global Data Assimilation System. *Mon Wea. Rev*., 134, 2612-2631.

Phalippou, L., 1996: A variational retrieval of humidity profile, wind speed and cloud liquid-water path with the SSM/I: Potential for numerical weather prediction. *Quart. J. Roy. Meteor. Soc.*, 122, 327-355.

Pu, Z. and W.-K. Tao, 2004: Mesoscale assimilation of TMI rainfall data with 4DVAR: Sensitivity studies. *J. Meteor. Soc. Japan*, 82, 1389-1397.

Putman W. M., and M. Suarez, 2011: Cloud-system resolving simulations with the NASA Goddard Earth Observing System global atmospheric model (GEOS-5). *Geophysical Research Letter*, Vol. 38, L16809, doi:10.1029/2011GL048438.

Randall, D. A., M. F. Khairoutdinov, A. Arakawa, and W. W. Grabowski, 2003: Breaking the cloud-parameterization deadlock. *Bull. Amer. Meteor. Soc*., 84, 1547-1564.

Skamarock, W. C. J. B. Klemp, J. Dudhia, D. O. Gill, D. M. Barker, W. Wang, and J. G. Powers, 2005: A description of the advanced research WRF version 2. NCAR Tech. Note NCAR/T-468+STR, 88pp.

Spencer, R. W., H. M. Goddman, and R. E Hood, 1989: Precipitation retrieval over land and ocean with the SSM/I. Part I: Identification and characteristics of the scattering signal. *J. Atmos. Oceanic Technol*., 6, 254-273.

Tao, W.-K., 2003: Goddard Cumulus Ensemble (GCE) model: Application for understanding precipitation processes. *Cloud Systems, Hurricanes, and the Tropical Rainfall Measuring Mission (TRMM): A Tribute to Dr. Joanne Simpson,* Meteor. Monogr., No. 51, Amer. Meteor. Soc., 103-108.

Tao, W.-K, and co-authors, 2008: A multiscale modeling system: Developments, applications, and critical issues. *Bull. Amer. Meteor. Soc*., 90, 515-534.

Treadon, R. E., 1996: Physical initialization in the NMC global data assimilation system. *Meteor. Atmos. Phys*., 60, 57-86.

Treadon, R. E., H.-L. Pan, W.-S. Wu, Y. Lin, W. Olson, and R. Kuligowski, 2002: Global and regional moisture analyses at NCEP. *Proc. ECMWF/GEWEX Workshop on Humidity Analysis*, Reading, United Kingdom, ECMWF, 33-47.

Tsuyuki, T., 1996a: Variational data assimilation in the Tropics using precipitation data. Part I: Column model. *Meteor. Atmos. Phys*., 60, 87-104.

Tsuyuki, T., 1996b: Variational data assimilation in the Tropics using precipitation data. Part II: 3D model. *Mon. Wea. Rev*., 124, 2545-2561.

Tsuyuki, T., 1997: Variational data assimilation in the Tropics using precipitation data, Part III: Assimilation of SSM/I precipitation rates. *Mon. Wea. Rev*., 125, 1447-1464.

Tsuyuki, T., K Koizumi, and Y. Ishikawa, 2002: The JMA Mesoscale 4DVAR System and assimilation of precipitation and moisture data. *Proc. ECMWF/GEWEX Workshop on Humidity Analysis*, Reading, United Kingdom, ECMWF, 59-67.

Weng, F., T. Zhu, and B. Yan, 2007: Satellite data assimilation in numerical weather prediction models. Part II: Uses of rain-affected radiances from microwave observations for hurricane vortex analysis. *J. Atmos. Sci*., 64, 3910-3925.

Wilheit, T. T., 1986: Some comments on passive microwave measurement of rain. *Bull. Amer. Meteor. Soc*., 67, 1226-1232.

Wilheit, T. T., C. Kummerow, and R. Ferraro, 2003: Rainfall algorithms for AMSR-E. *IEEE Trans. Geosci. Remote Sens*., 41, 204-213.

Wu, W.-S., R. J. Purser, and D. F. Parrish, 2002: Three-dimensional variational analysis with spatially inhomogeneous covariances. *Mon. Wea. Rev*., 130, 2905-2916

Xiao, Q., X. Zou, and Y.-H. Kuo, 2000: Incorporating the SSMI-derived precipitable water and rainfall rate into a numerical model: A case study for the ERICA IOP-4 cyclone. *Mon. Wea. Rev*., 128, 87-108.

Yuter, S. E., and R. A. Houze, Jr., 1995: Three-dimensional kinematic and microphysical evolution of Florida cumulonimbus. Part II: Frequency distribution of vertical velocity, reflectivity, and differential reflectivity. *Mon. Wea. Rev*., 123, 1941-1963.

Zhang, J., K. Howard, C. Langston, S. Vasiloff, B. Kaney, A. Arthur, S. V. Cooten, K. Kelleher, D. Kitzmiller, F. Ding, D.-J. Seo, Ernie Wells, C. Dempsey, 2011: National Moasic and Multi-Sensor QPE (NMQ) System: Description, results, and future plans. *BAMS*, 92, 1321-1338.

Zhang, S. Q., M. Zupanski, A. Y. Hou, X. Lin, and S. Cheung, 2013: Assimilation of precipitation-affected radiances in a cloud-resolving WRF ensemble data assimilation system. *Mon. Wea. Rev*., 141, 754-772.

Zupanski, M., 2005: Maximum likelihood ensemble filter: Theoretical aspects. *Mon. Wea. Rev.*, 133, 1710-1726.

Zupanski, M., I. M. Navon, and D. Zupanski, 2008: The maximum likelihood ensemble filter as a non-differentiable minimization algorithm. *Quart. J. Roy. Meteor. Soc*., 134, 1039-1050.

Zupanski, D., S. Q. Zhang, M. Zupanski, A. Y. Hou, and S. H. Cheung, 2011: A prototype WRF-based ensemble data assimilation system for dynamically downscaling satellite precipitation observations. *J. Hydrometeorology*, 12, 118-134.

# List of Figures

gauge precipitation (in mm/hr.) and VIRS cloud-top temperature (in K): (1) TMI BT > 270 K; (2) 250 K < TMI BT < 270 K; (3) 230 K < TMI BT < 250 K; (4) TMI BT < 230 K. The dashed line and the dotted line in the horizontal represent the 0°C and -20°C levels.

Figure 7: Accumulations (log10 (counts)) of different FGS 85 GHz radiance ensembles over the area where observations indicate rain on jointed histograms of surface radar-gauge precipitation (in mm/hr.) and FGS cloud-top temperature (in K): (1) FGS BT > 270 K; (2) 250 K < FGS BT < 270 K; (3) 230 K < FGS BT < 250 K; (4) FGS BT < 230 K. The dashed line and the dotted line in the horizontal represent the 0°C and -20°C levels.

Figure 8: Differences between the model analysis and the model first guess over the area where observations indicate rain on jointed histograms of surface radar-gauge precipitation (in mm/hr.) and model cloud-top temperature (in K): (1) BT > 270 K; (2) 250 K < BT < 270 K; (3) 230 K < BT < 250 K; (4) BT < 230 K. The dashed line and the dotted line in the horizontal represent the 0°C and -20°C levels..

Figure 9: Jointed histograms of 85 GHz radiances (K): (a) TMI; (b) First-guess (FGS); (c) Analysis (ANA); (d) Analysis minus First-guess, vs. Stage IV rain rate (mm/hr.) over regions where FGS indicates rain but observations show non-zero rain.

Figure 10: Accumulations (log10 (counts)) of different TMI 85 GHz radiance ensembles over the area where FGS indicates rain but observations show zero rain on jointed

histograms of surface radar-gauge precipitation (in mm/hr.) and FGS cloud-top temperature (in K): (1) TMI BT > 270 K; (2) 250 K < TMI BT < 270 K; (3) 230 K < TMI BT < 250 K; (4) TMI BT < 230 K. The dashed line and the dotted line in the horizontal represent the 0°C and -20°C levels.

Figure 11: Accumulations (log10 (counts)) of different FGS 85 GHz radiance ensembles over the area where FGS indicates rain but observations show zero rain on jointed histograms of surface radar-gauge precipitation (in mm/hr.) and FGS cloud-top temperature (in K): (1) FGS BT > 270 K; (2) 250 K < FGS BT < 270 K; (3) 230 K < FGS BT < 250 K; (4) FGS BT < 230 K. The dashed line and the dotted line in the horizontal represent the 0°C and -20°C levels.

Figure 12: Differences between the model analysis and the model first guess over the area where FGS indicates rain but observations show zero rain on jointed histograms of surface radar-gauge precipitation (in mm/hr.) and model cloud-top temperature (in K): (1) BT > 270 K; (2) 250 K < BT < 270 K; (3) 230 K < BT < 250 K; (4) BT < 230 K. The dashed line and the dotted line in the horizontal represent the 0°C and -20°C levels.

Figure 13: CFADs of S-band radar vertical reflectivity profiles over areas where observations indicate rain for observations, FGS, ANA, and (ANA-FGS). The dashed line and the dotted line in the horizontal represent the 0°C and -20°C levels.

Figure 14: CFADs of S-band radar vertical reflectivity profiles over areas where the model forecast indicates rain but the observation does not. The dashed line and the dotted line in the horizontal represent the 0°C and -20°C levels.

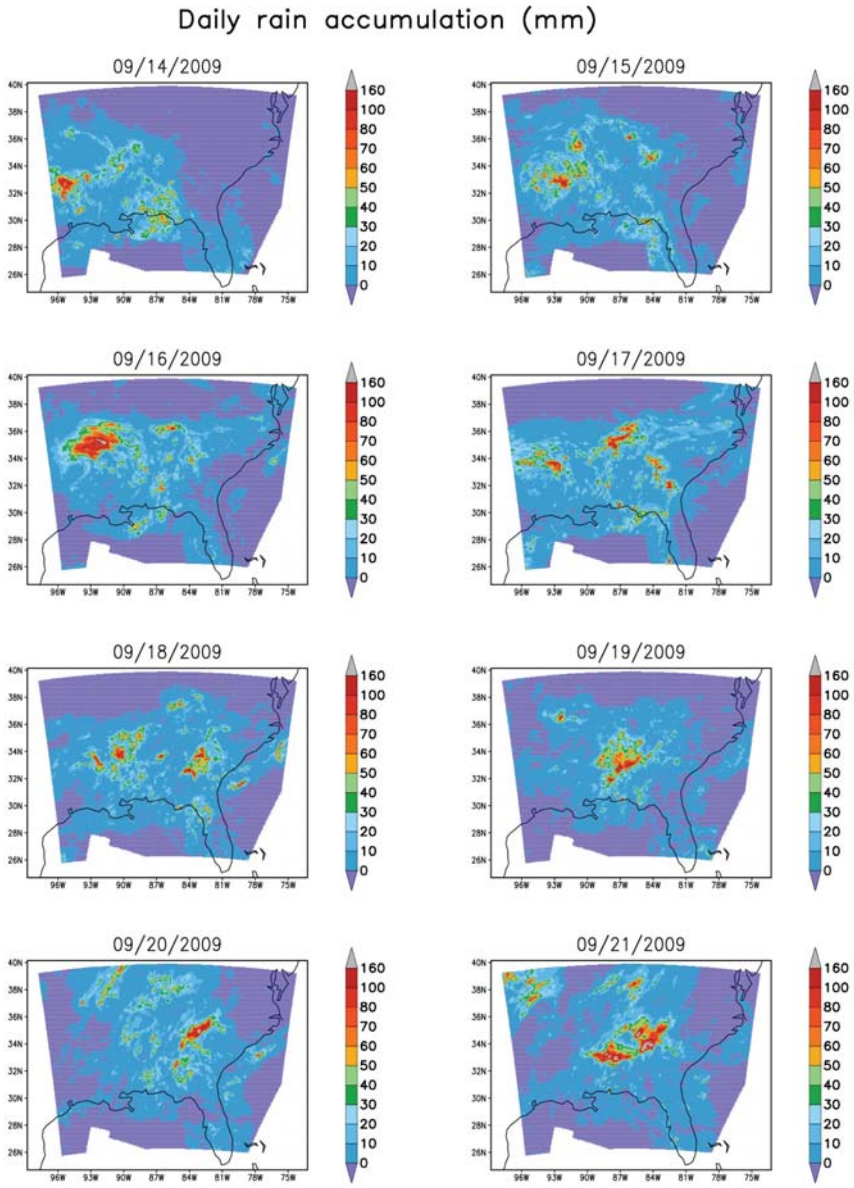


Figure 1: Daily rain accumulation (mm) over the WRF-EDAS experiment domain from 09/14/2009 to 09/21/2009 as derived from the Stage IV hourly surface radar-gauge merged analysis.

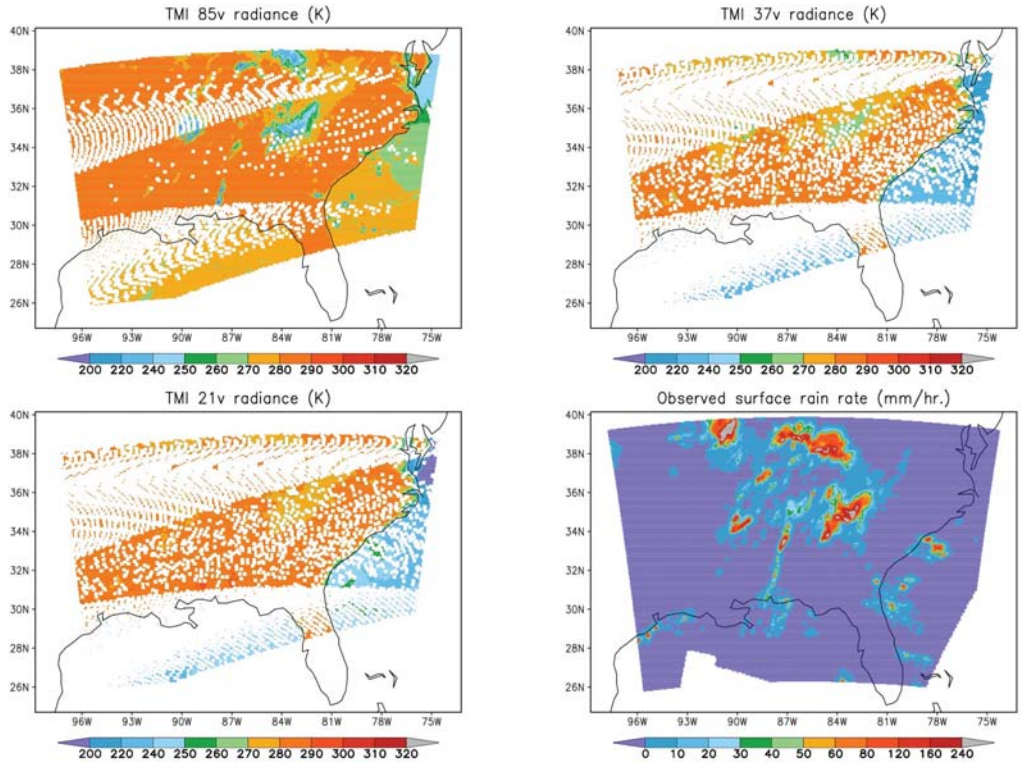


Figure 2: Snapshots of the TMI 85 GHz (V), 37 GHz (V) and 21 GHz (V) overpasses centered at 15Z, September 20, 2009 within the WRF-EDAS experiment domain, along with the observed surface rain rate from ground radar and gauge observations.

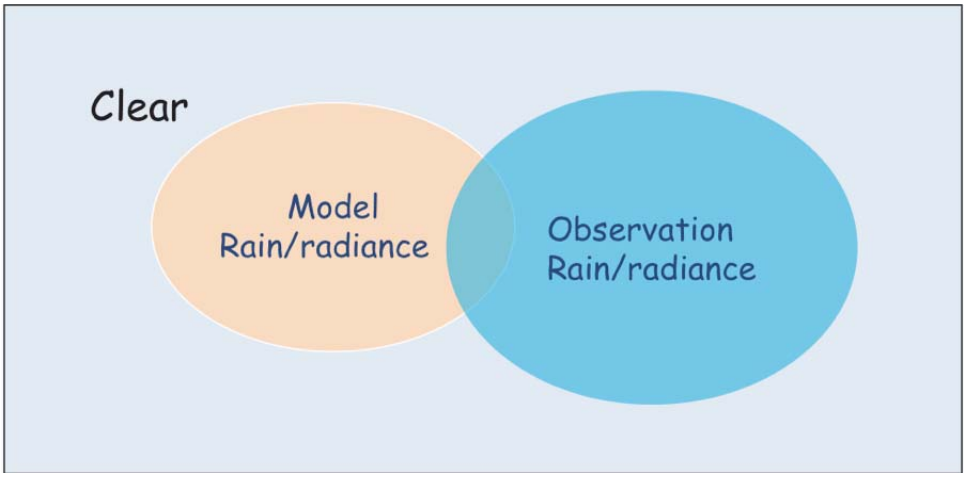


Figure 3: A schematic showing a typical scene in which the observation and model forecast have mismatches in terms of area coverage of precipitation-affected radiance.

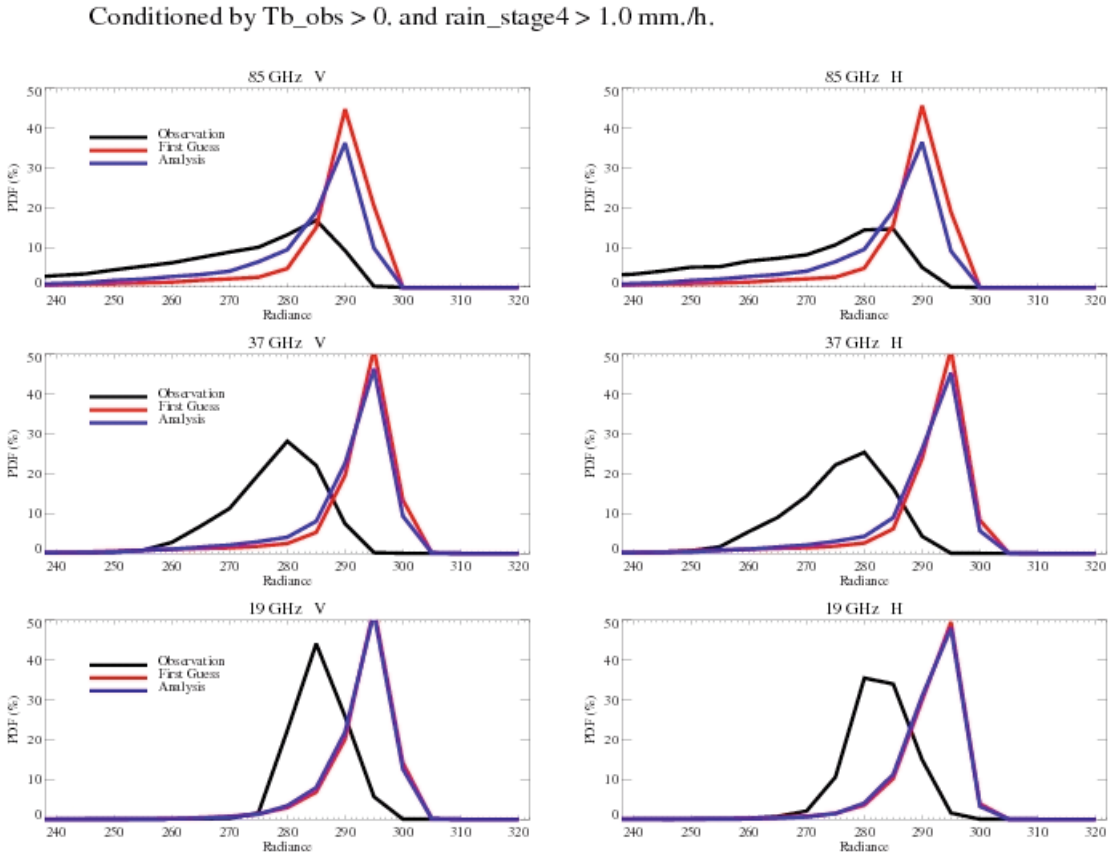


Figure 4: Histograms of radiances at 85 GHz, 37 GHz, and 19 GHz from TRMM TMI (black), model forecast (first guess, red), and analysis (purple) over areas where observed surface rain rates are larger than 1.0 mm/hr.

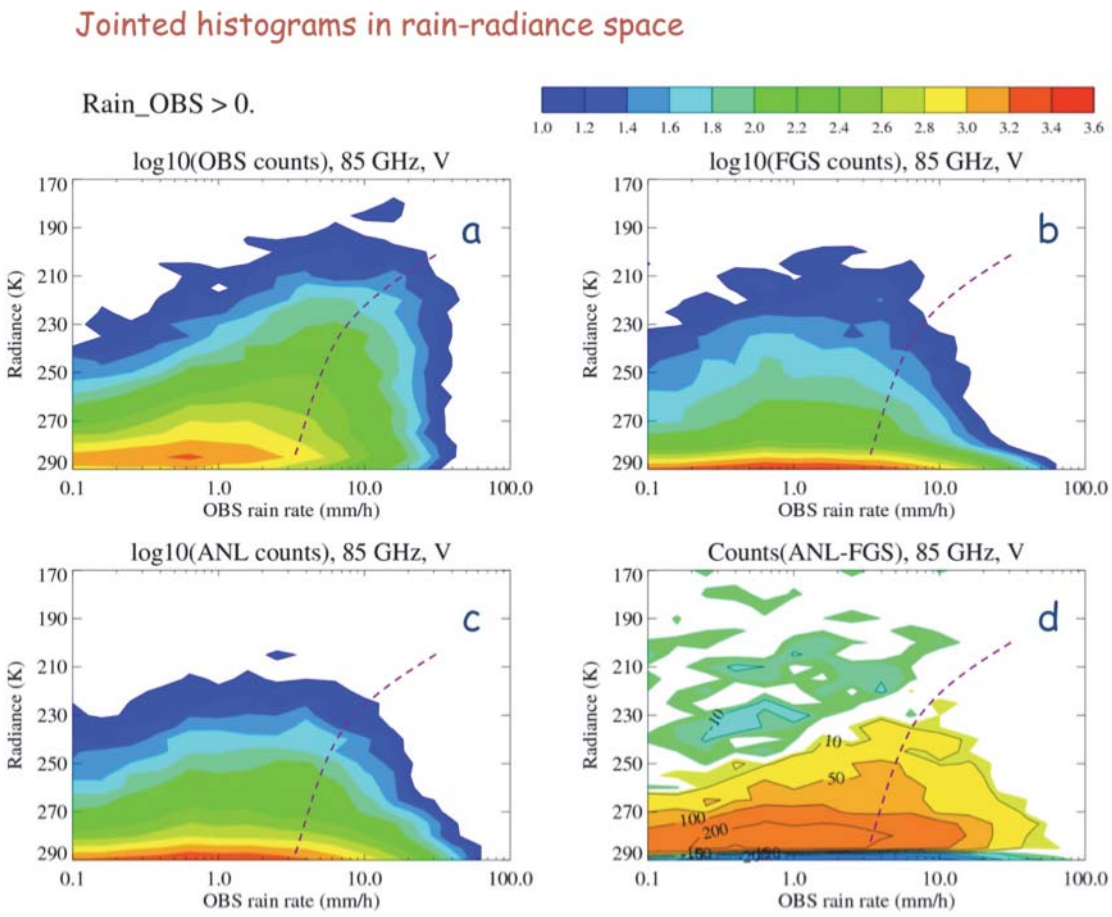


Figure 5: Jointed histograms of 85 GHz radiances (K): (a) TMI; (b) First-guess (FGS); (c) Analysis (ANA); (d) Analysis minus First-guess, vs. Stage IV rain rate (mm/hr.) over regions where observations indicate non-zero rain rates. The dashed line indicates the largest gradient between TMI 85 GHz radiance and observed surface rain rate.

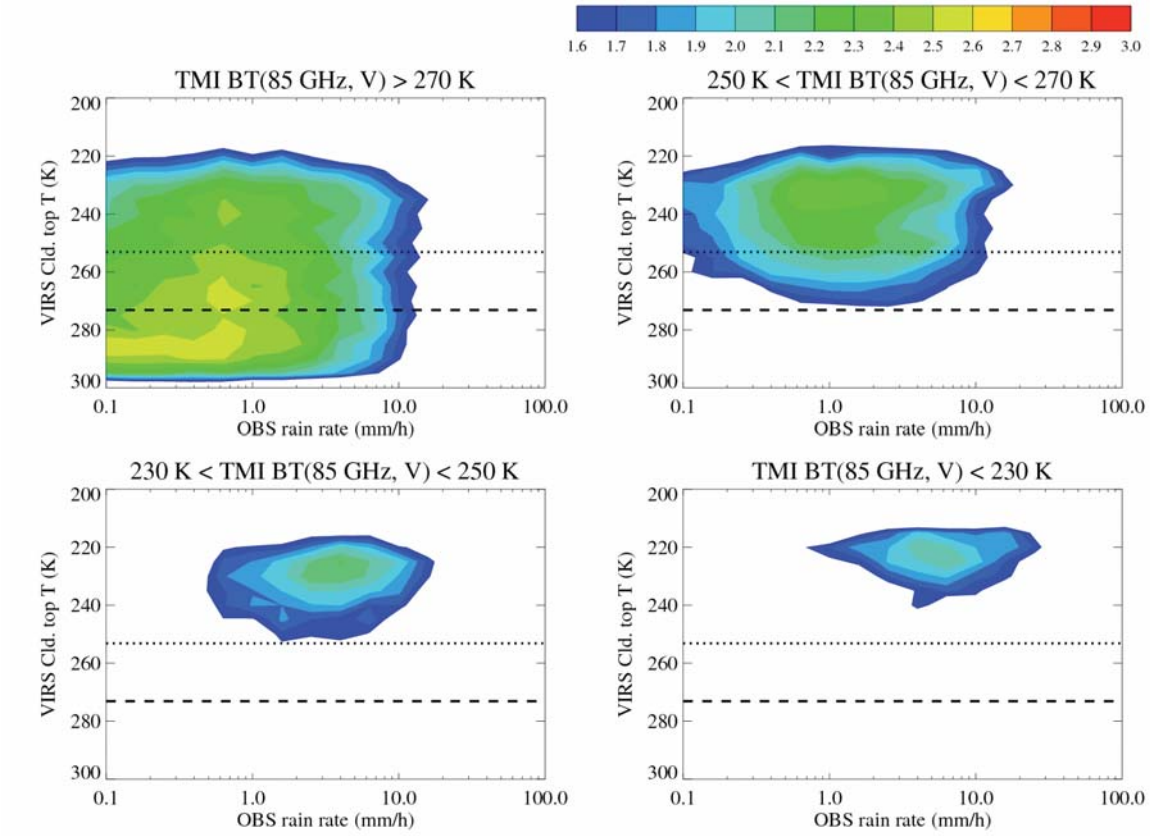


Figure 6: Accumulations (log10 (counts)) of different TMI 85 GHz radiance ensembles over the area where observations indicate rain on jointed histograms of surface radar-gauge precipitation (in mm/hr.) and VIRS cloud-top temperature (in K): (1) TMI BT > 270 K; (2) 250 K < TMI BT < 270 K; (3) 230 K < TMI BT < 250 K; (4) TMI BT < 230 K. The dashed line and the dotted line in the horizontal represent the 0°C and -20°C levels.

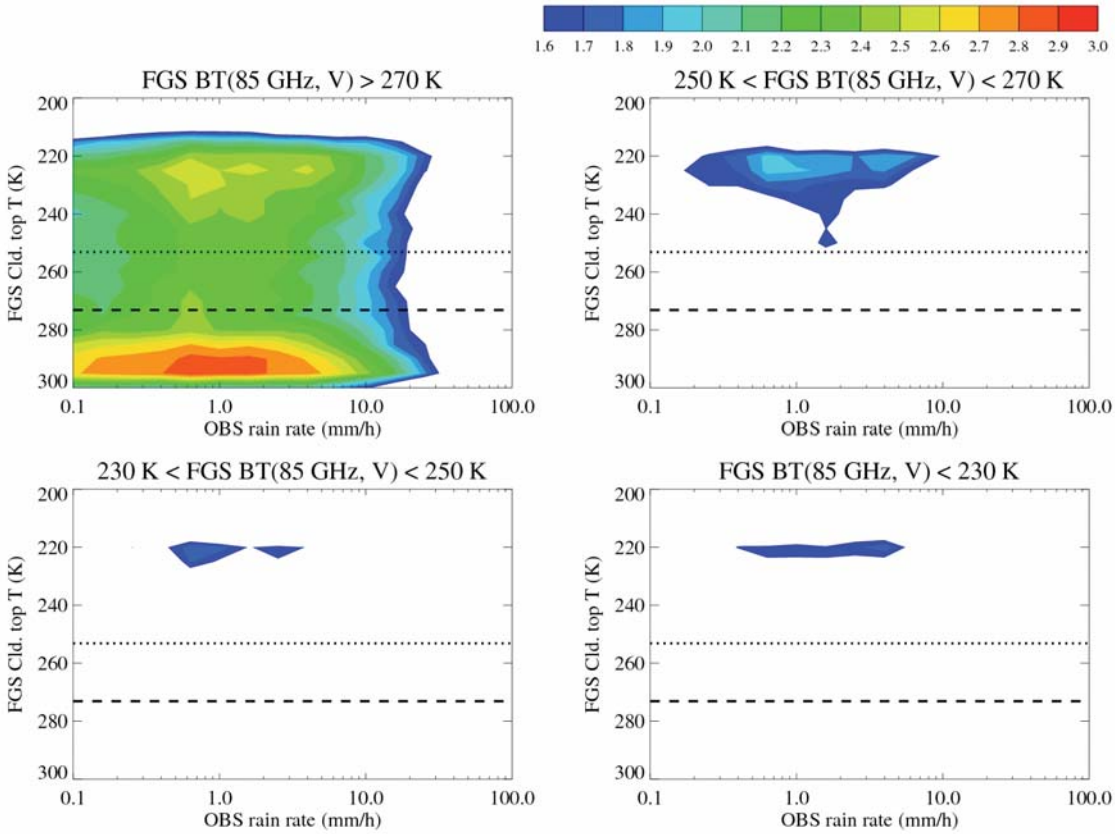


Figure 7: Accumulations (log10 (counts)) of different FGS 85 GHz radiance ensembles over the area where observations indicate rain on jointed histograms of surface radar-gauge precipitation (in mm/hr.) and FGS cloud-top temperature (in K): (1) FGS BT > 270 K; (2) 250 K < FGS BT < 270 K; (3) 230 K < FGS BT < 250 K; (4) FGS BT < 230 K. The dashed line and the dotted line in the horizontal represent the 0°C and -20°C levels.

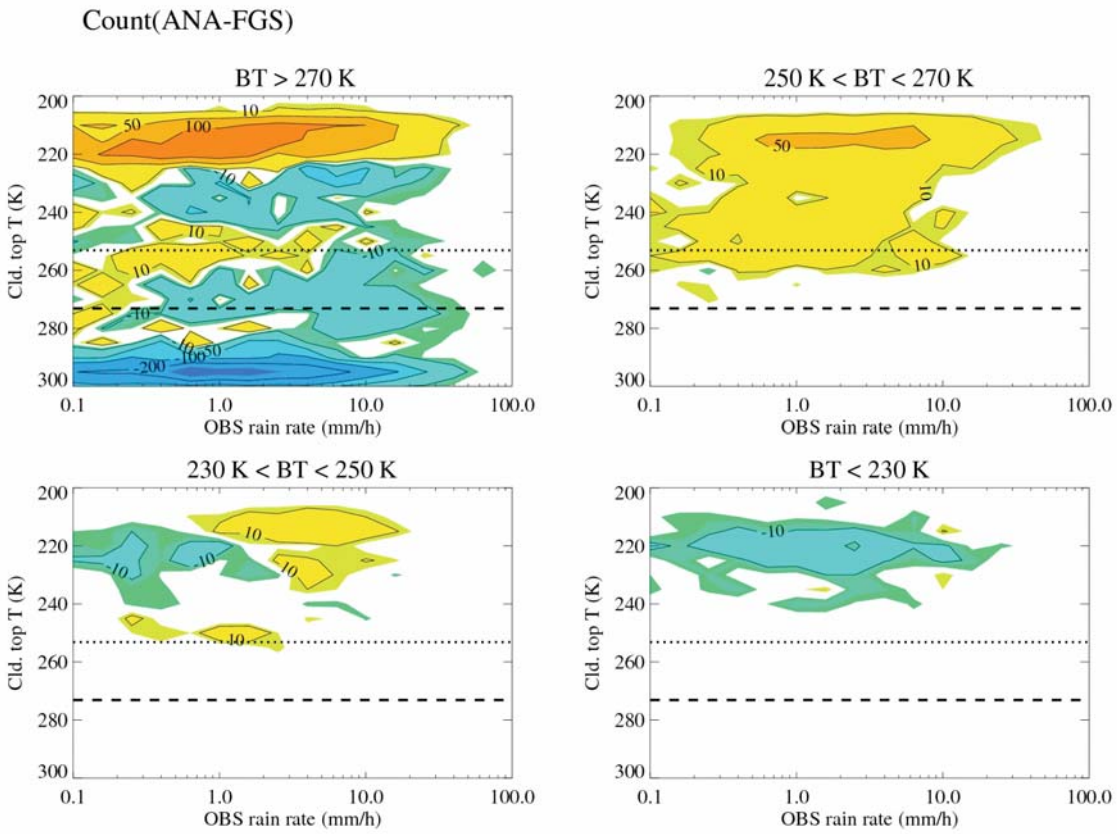


Figure 8: Differences between the model analysis and the model first guess over the area where observations indicate rain on jointed histograms of surface radar-gauge precipitation (in mm/hr.) and model cloud-top temperature (in K): (1) BT > 270 K; (2) 250 K < BT < 270 K; (3) 230 K < BT < 250 K; (4) BT < 230 K. The dashed line and the dotted line in the horizontal represent the 0°C and -20°C levels.

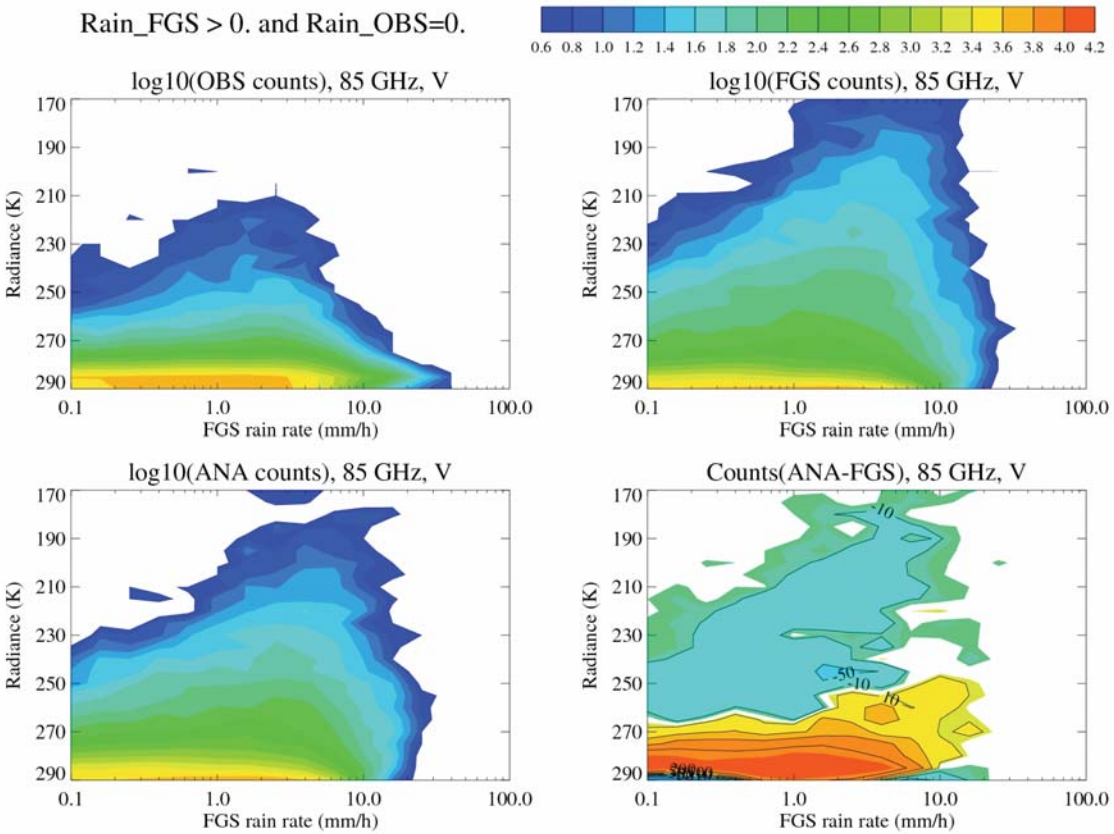


Figure 9: Jointed histograms of 85 GHz radiances (K): (a) TMI; (b) First-guess (FGS); (c) Analysis (ANA); (d) Analysis minus First-guess, vs. Stage IV rain rate (mm/hr.) over regions where FGS indicates rain but observations show non-zero rain.

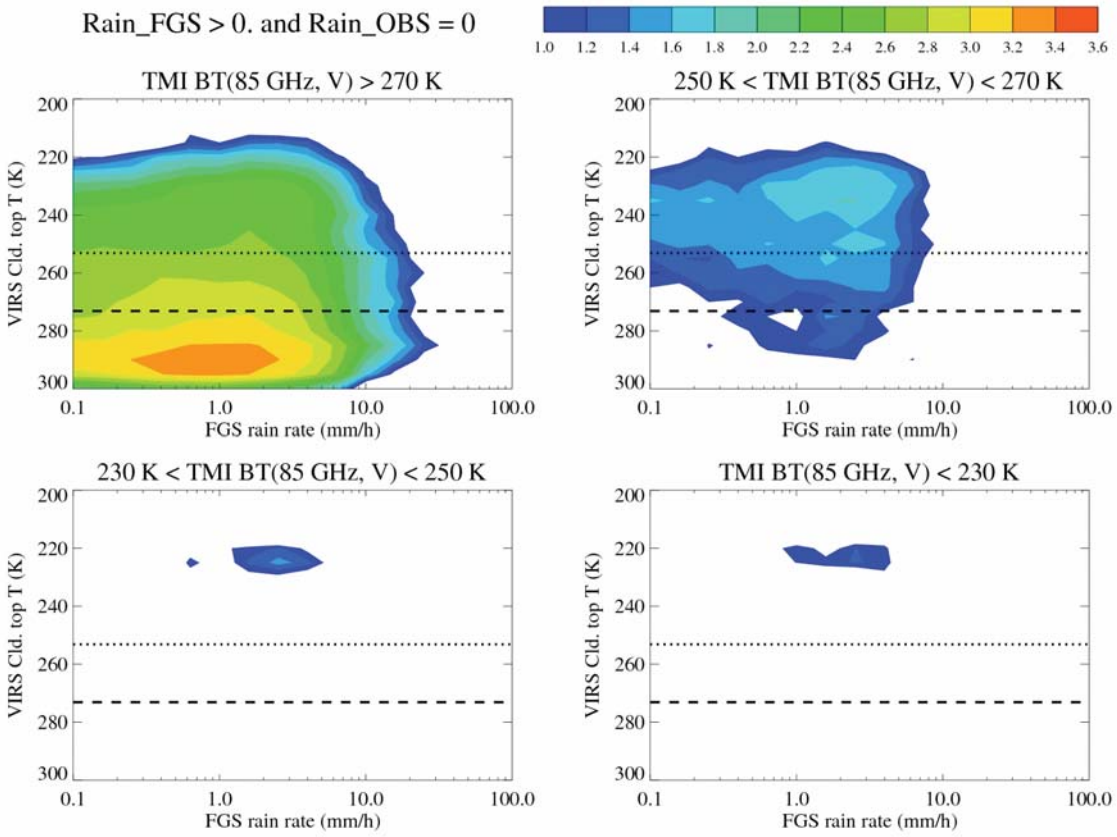


Figure 10: Accumulations (log10 (counts)) of different TMI 85 GHz radiance ensembles over the area where FGS indicates rain but observations show zero rain on jointed histograms of surface radar-gauge precipitation (in mm/hr.) and FGS cloud-top temperature (in K): (1) TMI BT > 270 K; (2) 250 K < TMI BT < 270 K; (3) 230 K < TMI BT < 250 K; (4) TMI BT < 230 K. The dashed line and the dotted line in the horizontal represent the 0°C and -20°C levels.

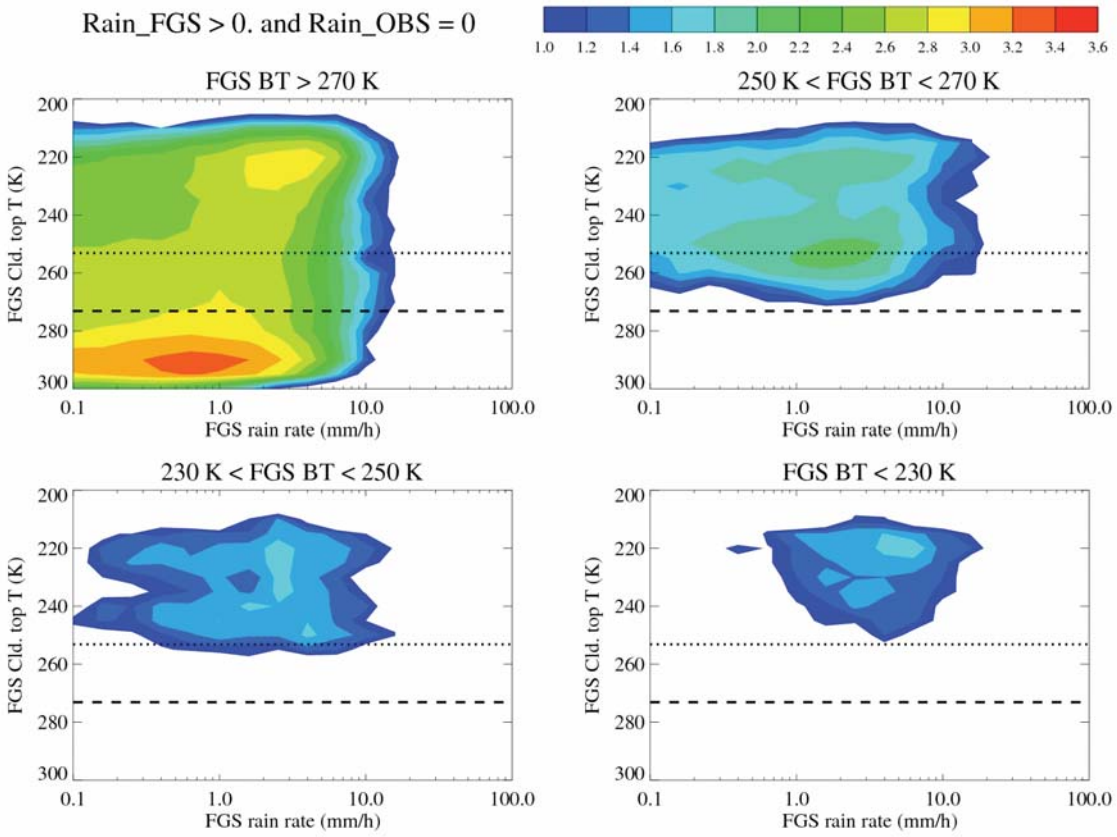


Figure 11: Accumulations (log10 (counts)) of different FGS 85 GHz radiance ensembles over the area where FGS indicates rain but observations show zero rain on jointed histograms of surface radar-gauge precipitation (in mm/hr.) and FGS cloud-top temperature (in K): (1) FGS BT > 270 K; (2) 250 K < FGS BT < 270 K; (3) 230 K < FGS BT < 250 K; (4) FGS BT < 230 K. The dashed line and the dotted line in the horizontal represent the 0°C and -20°C levels.

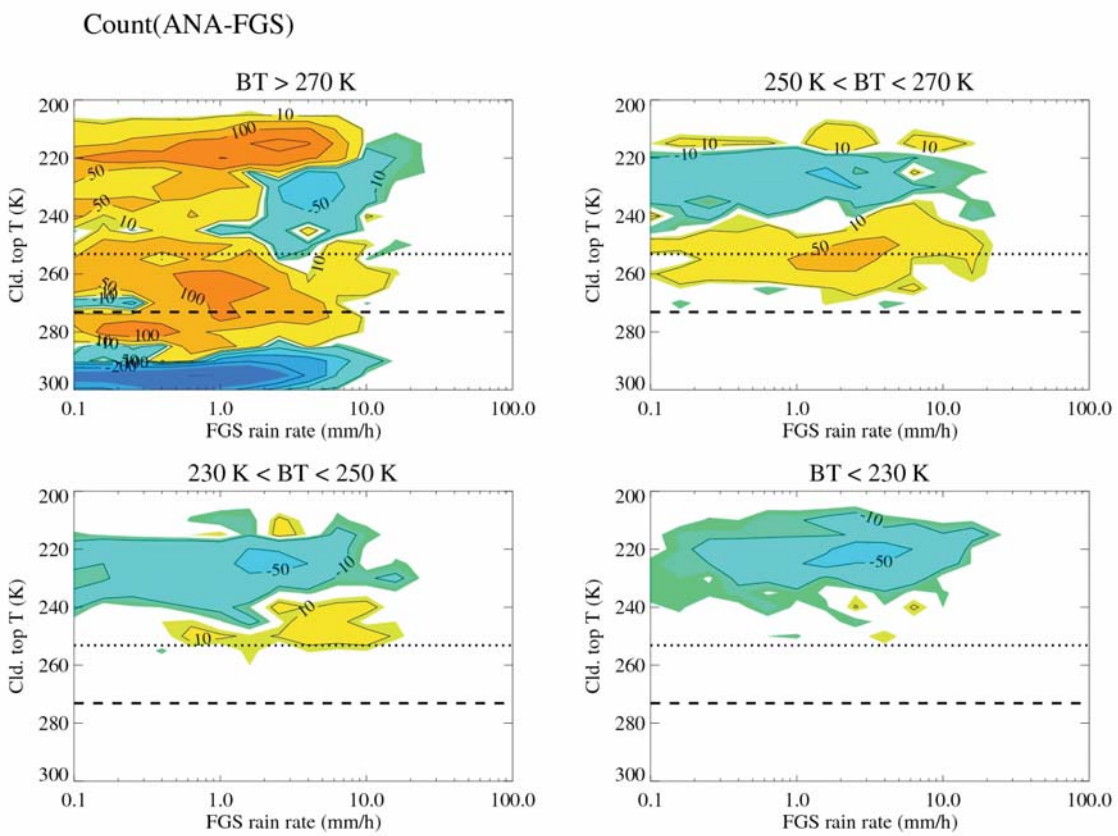


Figure 12: Differences between the model analysis and the model first guess over the area where FGS indicates rain but observations show zero rain on jointed histograms of surface radar-gauge precipitation (in mm/hr.) and model cloud-top temperature (in K): (1) BT > 270 K; (2) 250 K < BT < 270 K; (3) 230 K < BT < 250 K; (4) BT < 230 K. The dashed line and the dotted line in the horizontal represent the 0°C and -20°C levels.

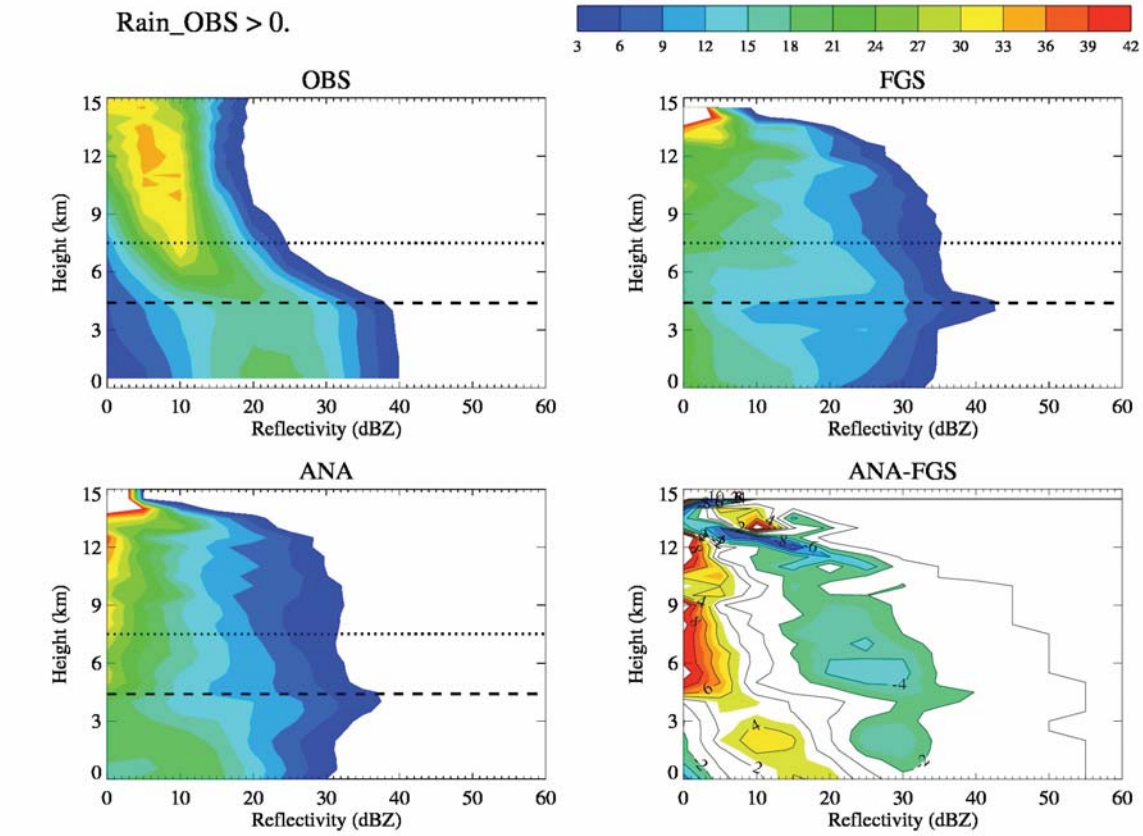


Figure 13: CFADs of S-band radar vertical reflectivity profiles over areas where observations indicate rain for observations, FGS, ANA, and (ANA-FGS). The dashed line and the dotted line in the horizontal represent the 0°C and -20°C levels.

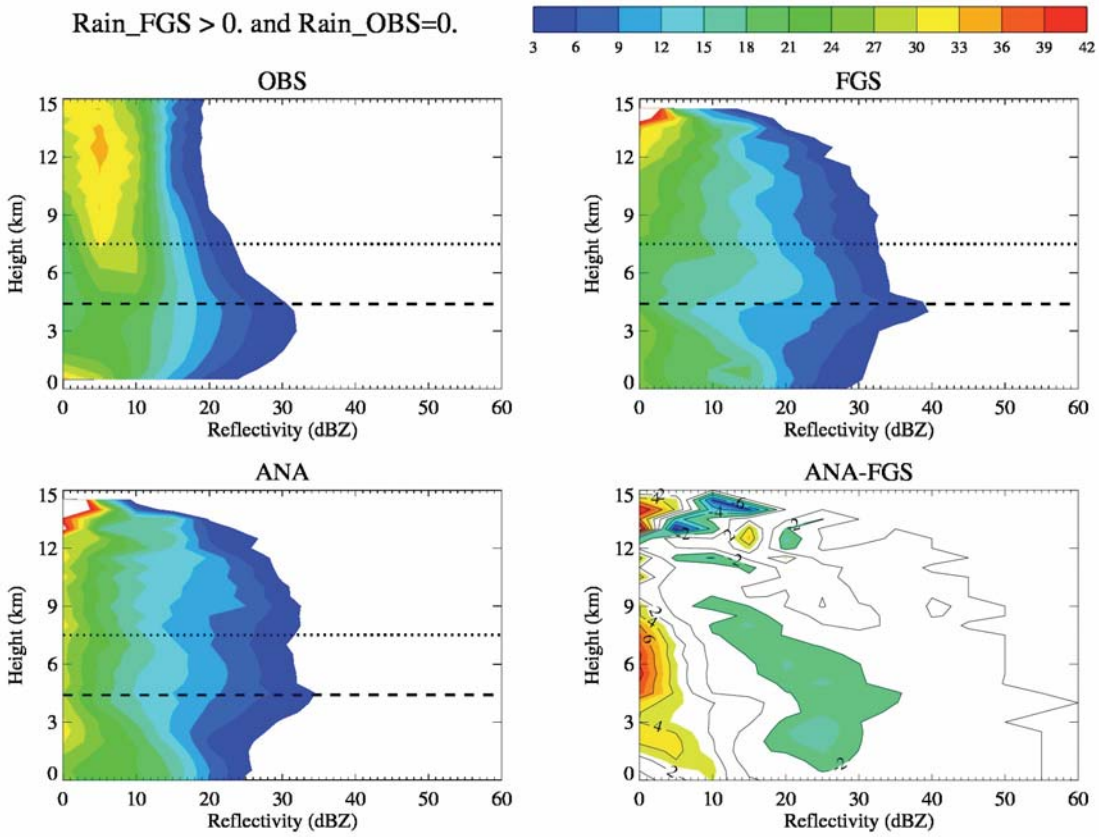


Figure 14: CFADs of S-band radar vertical reflectivity profiles over areas where the model forecast indicates rain but the observation does not. The dashed line and the dotted line in the horizontal represent the 0°C and -20°C levels.